Investigating the Potential of Multisequence Displacement Timeseries for Fault Rheology Estimation

Tobias Köhne[1], Rishav Mallick[2], and Mark Simons[2]

[1]California Institute of Technology Division of Geological and Planetary Sciences
[2]California Institute of Technology

January 27, 2023

Abstract

Understanding the nature and behavior of the rocks in boundary zones between tectonic plates is important to improve our understanding of earthquake-associated hazard. Laboratory experiments can derive models that explain material behavior on small scales and under controlled conditions. These models can also be tested on observations of surface motion near plate boundaries: Fitting surface displacements from earthquakes (either shortterm offsets or longterm motion) yields estimates of rock properties for each model. However, using only observations from a single earthquake (from immediately after the quake and/or the subsequent years), may not allows us to confidently distinguish between models. In this study, we investigate the potential of using the displacement timeseries from multiple earthquakes, as well as the period between the quakes, to distinguish between proposed models. We use methods that enable comparison between models and parameters taking into account uncertainties, and perform our assessment on an artificial dataset.

Investigating the Potential of Multisequence Displacement Timeseries for Fault Rheology Estimation

Tobias Köhne[1], Rishav Mallick[1], Mark Simons[1]

[1] Seismological Laboratory, Division of Geological and Planetary Sciences, California Institute of Technology

EARLY PRELIMINARY STATE OF WORK

About Me
tkoehne@caltech.edu
www.tobiaskoehne.de
AGU Fall Meeting 2022
T32E-0229

I. Motivation & Previous Work

- **Constraining the effective rheology of tectonic plate interfaces is crucial** to improve our understanding of the physics of plate boundary deformation (e.g., Bürgmann & Dresen, 2008) — including questions like **how does stress accumulate, release and distribute** during the earthquake cycle, where and how are mountain ranges sustained, how can plate-like tectonics exist, and what does our understanding imply for seismic hazard assessments?
- **Laboratory experiments** have been used to propose constitutive relations of specific rock types at the **micron to meter scale** (e.g., Blanpied et al., 1995; Hirth, 2002; Hirth & Kohlstedt, 2003).
- Postseismic displacement timeseries observations near plate interfaces have since been used to estimate ranges of parameters for such models (e.g., Freed et al., 2012; Agata et al., 2019; Muto et al., 2019; Weiss et al., 2019; Fukuda & Johnson, 2021) although it is unclear if **geodetic evidence** can distinguish between different models at **megathrust scales**.

→ **Longterm goal:** *Identify classes of rheological models that are internally consistent over different phases of the seismic cycle.*

- We build on the concepts of Hetland & Simons (2010) and Hetland et al. (2010) that **model interseismic creep in an idealized subduction zone** given a recurring rupture sequence, locked asperity patches, and a rheological model.

→ **Goal for this study:** *Develop a framework to solve for rheological parameters on a simulated, 2D megathrust in a probabilistic inverse sense, with the eventual aim of full 3D analysis of geodetic data in Northern Japan.*

II. Method

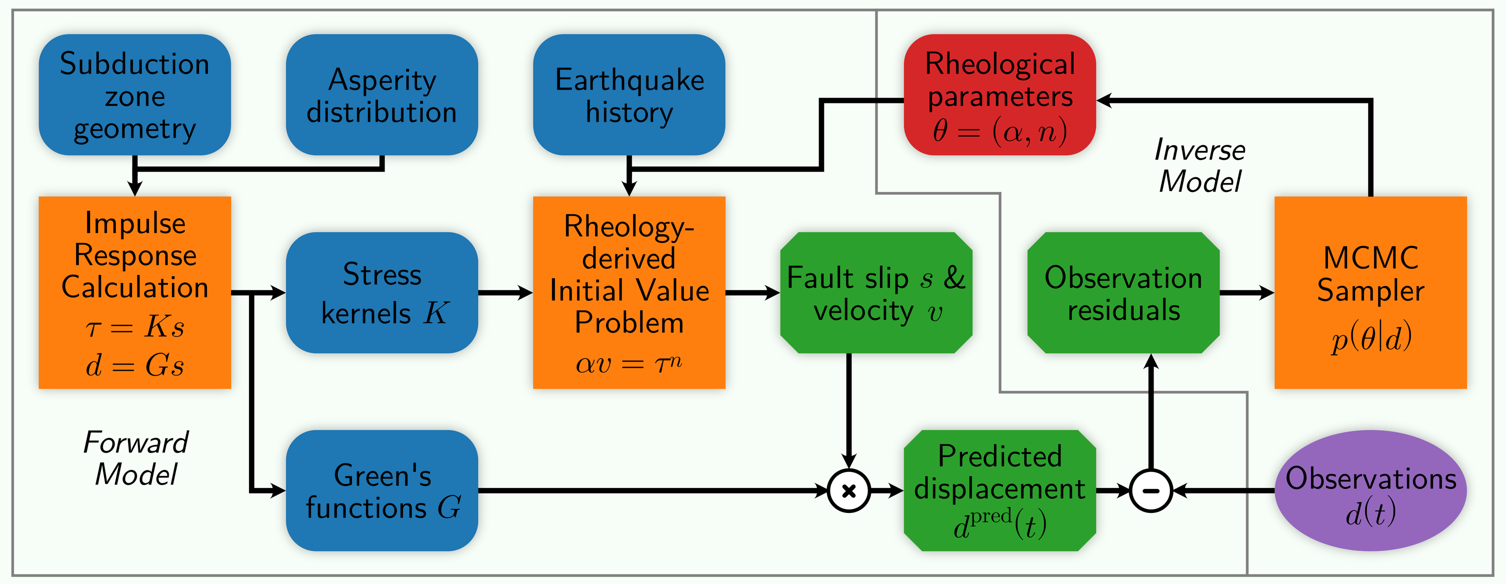

Fig. 1: Workflow schematic. Orange rectangles represent key computational steps. Rounded rectangles represent hyperparameters (kept constant) and regular parameters (to be estimated) in blue and red, respectively. Rectangles with cut corners represent state variables, and the purple ellipse represents the (synthetic) observations. More details about the process below.

Forward model:

- **Asperities: predefined regions that only slip coseismically** with known recurrence time and slip amount.
- **Rheology: depth-dependent power-law viscous rheology** $\alpha v = \tau^n$ (α rheological strength term, v slip velocity, τ shear stress, n power-law exponent), appropriate for linear-viscous, power-law viscous, and rate-dependent frictional models (e.g., Montési & Hirth, 2003; Montési, 2004; Mallick et al., 2022).
- **Boundary integral formulation:** $d\tau/dt = K(v - v_p)$ (K stress kernel, v_p plate velocity), initial conditions obtained by spin-up.

Inverse model:

- **Markov-Chain Monte-Carlo (MCMC) framework:** maximize the likelihood $p(d|\theta) = \mathcal{N}(d|g(\theta), C_X)$, matching the entire timeseries (not a functional fit), yielding the **posterior distribution** $\boldsymbol{p(\theta|d)}$ for parameters $\theta = (\alpha, n)$ using the CATMIP algorithm (Minson et al., 2013) as implemented in the AlTar software.
- **Errors:** observations $d = g(\theta) + e + \epsilon$, corrupted by observation errors e (covariance C_d currently assumed as constant, diagonal matrix) as well as the model errors ϵ (covariance C_p, currently ignored) with $C_X = C_d + C_p$.

III. Model Setup

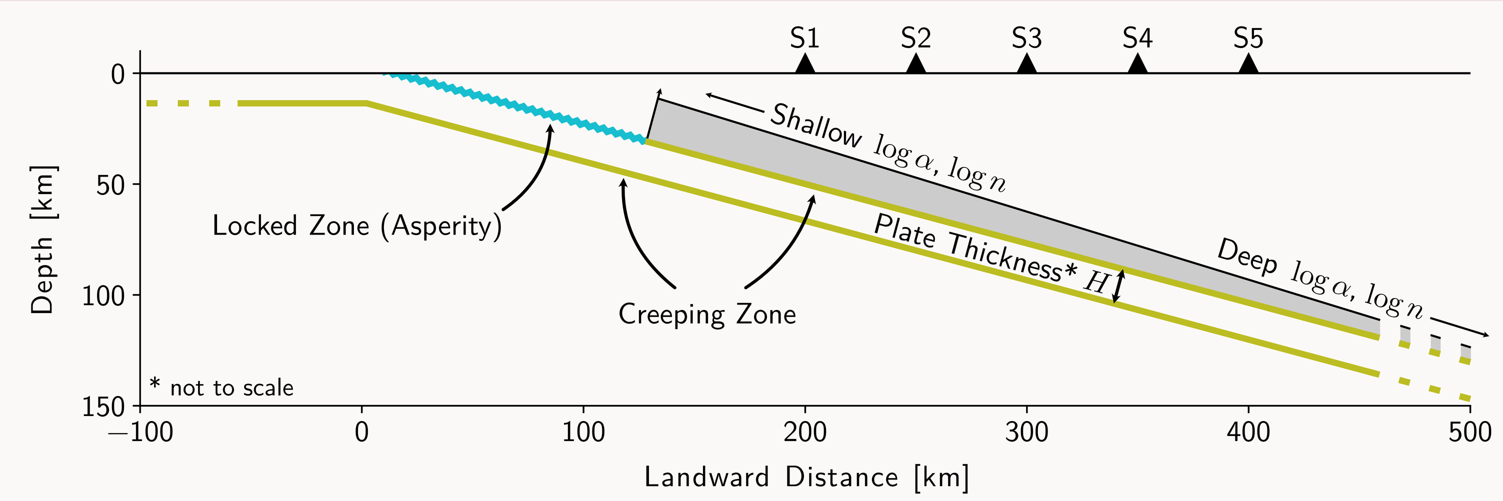

Fig. 2 (above): Model setup of the subduction zone, following the Elastic Subducting Plate Model (ESPM, Kanda & Simons, 2010). Two plate interfaces approximate the downgoing slab, with the upper and lower interface experiencing left- and right-lateral shearing motion, respectively. The location of observers S1–5 (Fig. 4) is given by the black triangles. Over the length of the upper, creeping interface (going down to 600 km depth, not shown here), the rheological parameters α and n vary linearly in logarithmic space.

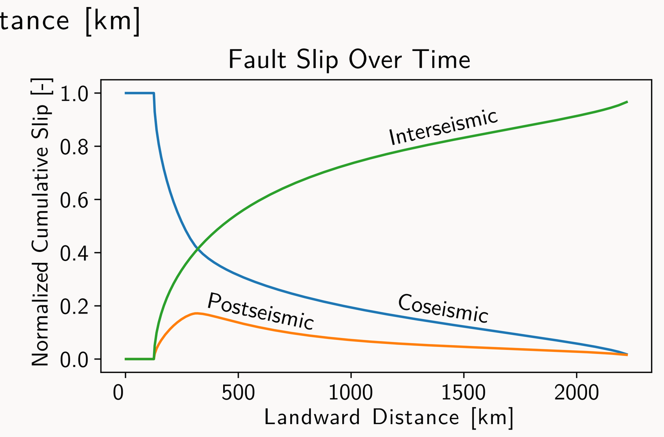

Fig. 3 (right): Cumulative slip on the locked and creeping fault patches for different timespans within the earthquake cycle, normalized by the total amount of slip occuring over the entire cycle. The coseismic period (blue line) includes the step offset imposed by the earthquake, both within the locked zone as well as in the creeping zone through tapered slip (to mitigate unphysical stress spikes). The postseismic period (orange) represents the cumulative slip for the first 1% of the recurrence time interval, and the interseismic period (green) the remaining slip.

V. Base Test Case (1): Inferring Rheological Parameters

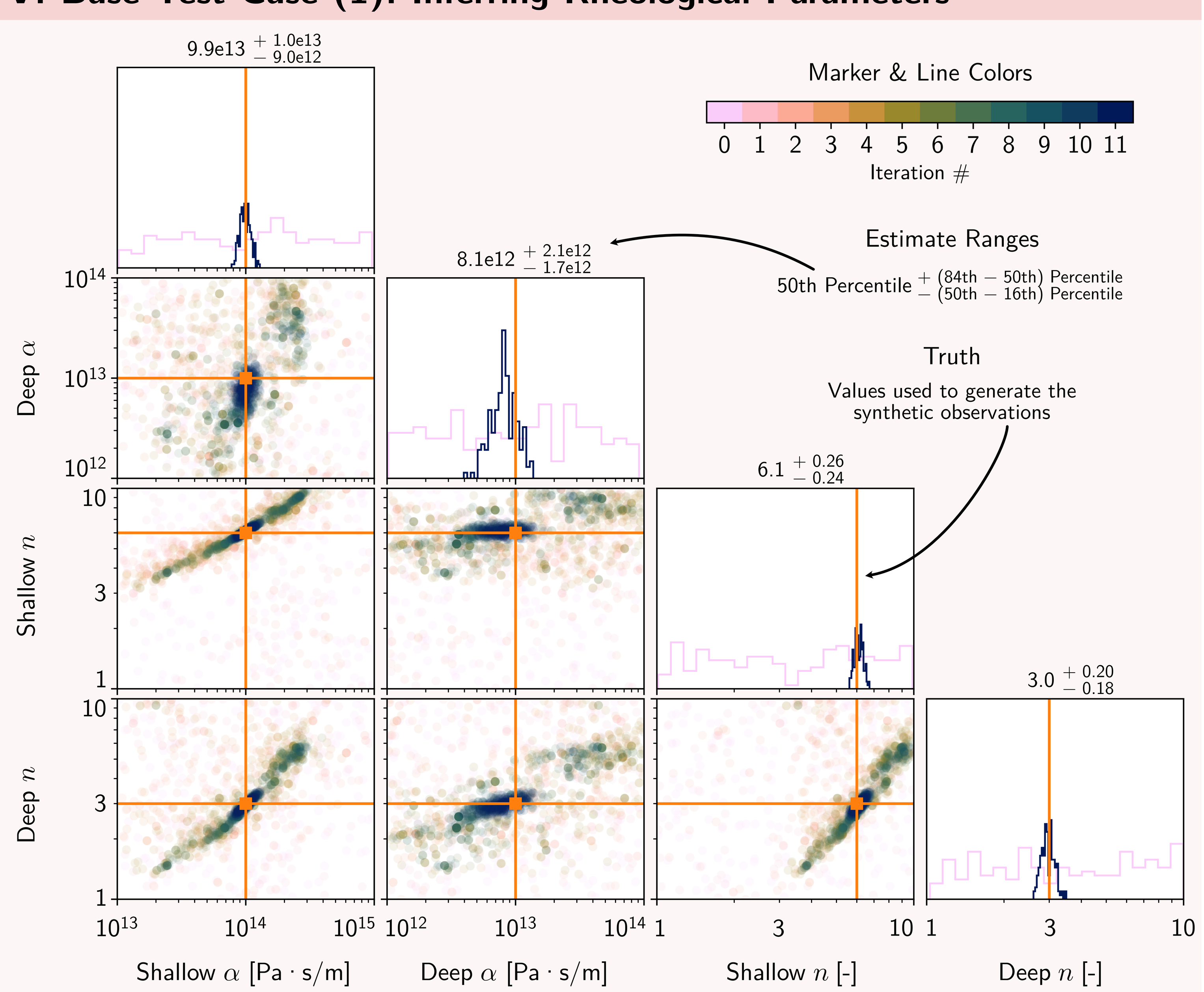

Fig. 5: Corner plot of the posterior covariance matrix as approximated by the MCMC inversion process for the two rheological parameters α and n at the shallow and deep ends of the creeping zone (modeled to vary linearly in logarithmic space between the boundaries). The figures on the diagonal represent 1D histograms of the marginalized probability density functions (PDF) for each parameter. In the off-diagonal plots, the MCMC samples at each iteration are plotted as circles, with their color indicating the iteration, to form a 2D histogram. From the convergence of the MCMC samples over successive iterations, as well as from the comparison of the prior and posterior marginal distributions in the 1D histograms, one can clearly see the recovery of the true parameters, as well as the strong correlations between each parameter. This test case completed in 10 minutes using 160 samples with a chain length of 5 using all 32 threads on a 16-core CPU.

IV. Synthetic Observations

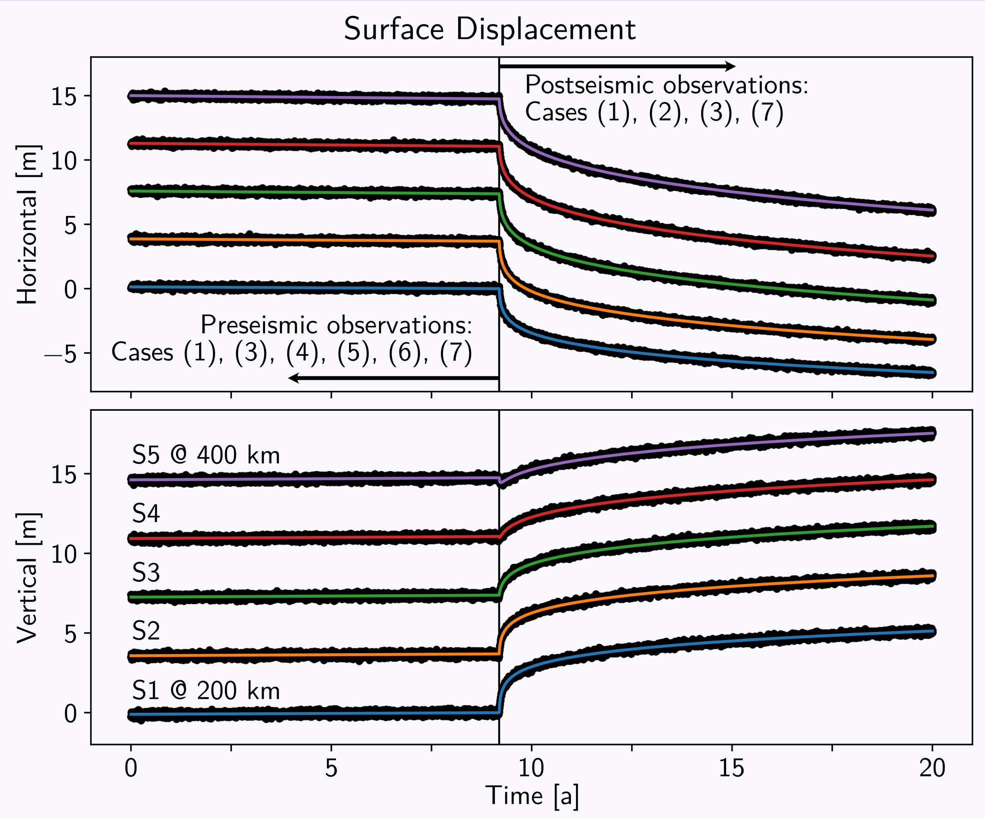

Fig. 4: Simulated surface displacement timeseries in both horizontal and vertical directions used as input for all test cases (see Fig. 5 for rheological parameters used to create this timeseries). The solid lines are the true timeseries, with colors corresponding to observer location. The labels refer to the names of the stations, with the range of trenchward distances given as well. The black dots are the synthetic observations which include a 10 cm standard deviation Gaussian noise. At approx. 9.2 a (vertical black line), an earthquake occurs and starts a postseismic transient process. The coseismic offset is removed both in this plot, as well as in the observations used in the inference process. Which observations a test case (see Fig. 6) uses is given by the text at the arrows indicating the pre- and postseismic phases.

VI. Exploring Inference Sensitivity

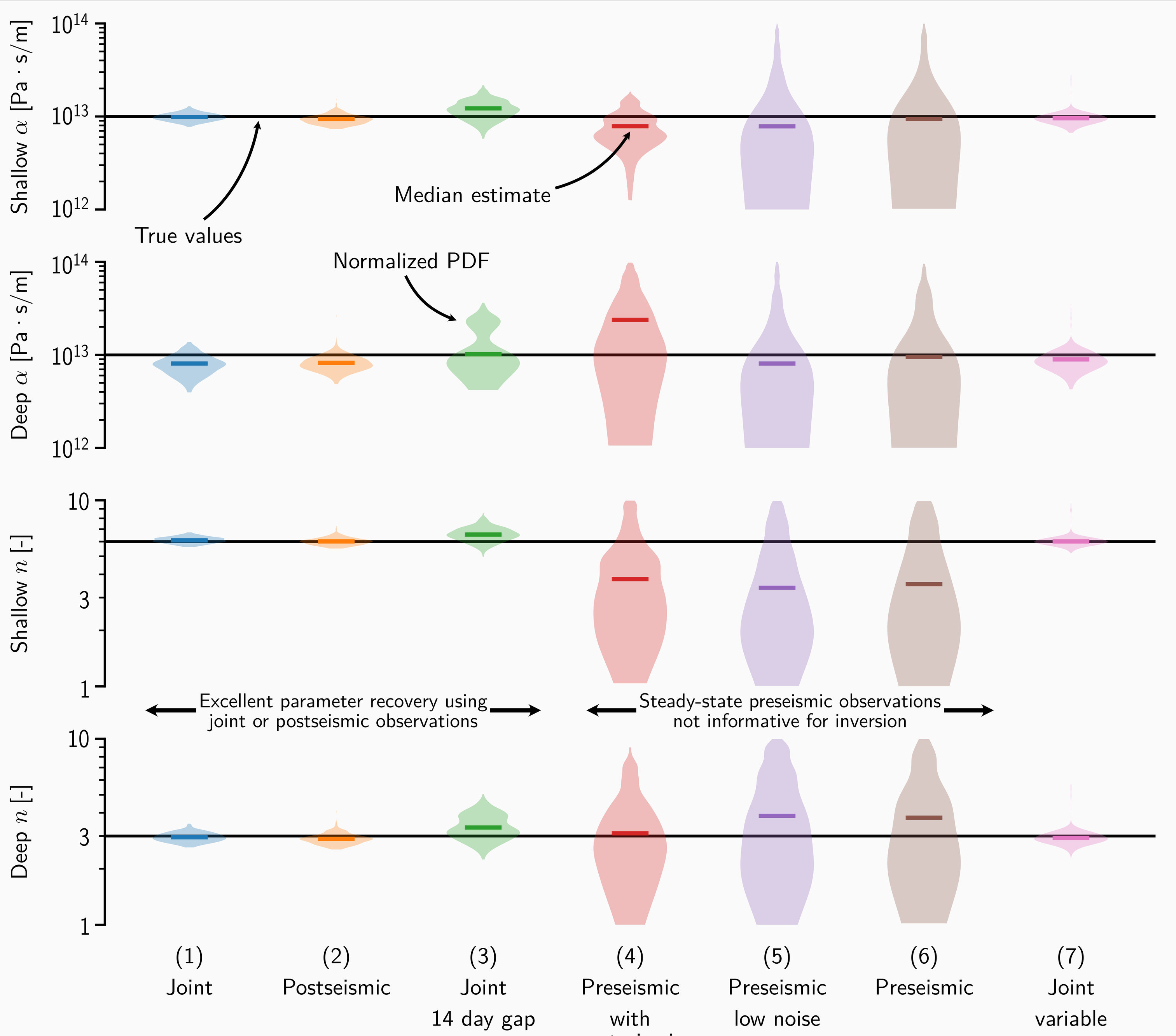

Fig. 6: Marginal posterior probability distributions of the four rheological parameters (see Fig. 5) for 7 different test cases, shown as violin plots. The shaded areas are normalized, smoothed vertical histograms, with the colored horizontal lines indicating the median estimates, and the black horizontal line indicating the true value. The different cases represent inversions with differing sets of observations. In the base case (1), presented in detail in Fig. 5, the inversion is informed by both pre- and postseismic surface displacement timeseries (see Fig. 4 for the available observations and timespans). In all cases, the coseismic offset is removed. In the inversion of case (2), only the postseismic observations are used. In case (3), preseismic observations and postseismic observations starting 14 days after the earthquake are used. Cases (4)–(6) only use preseismic observations. The timeseries in case (4), however, includes the tail of a smaller, unobserved earthquake. Case (5), in turn, only has a noise standard deviation of 1 mm. Case (6) uses the same preseismic observations as the base case. In case (7), we explore the effect of uncertainties in the recurrence time by allowing the recurrence time to vary by approx. ±10% (using both pre- and postseismic observations).

VII. Unmodeled Uncertainties

Our framework allows the exploration of uncertainties in our forward model in three ways:

- Moving a **hyperparameter** of the forward model **into the group of estimated parameters**, or
- **Sampling the hyperparameters from a distribution at each sample** of the forward model (without estimating it, increasing the posterior uncertainty), or
- Running the forward model with a variety of plausible hyperparameters, **calculating an empirical covariance** in data space, and incorporating it into the MCMC sampler as C_p.

Possible uncertainties to be explored are the timing of earthquakes, amount of coseismic slip, the fault geometry, and the removal of coseismic offsets.

VIII. Future Work

- Our principal next step is to **expand to a 3D domain and real data.**
- We aim to use the region of **Northern Japan** as our study example, because of the long & dense GNSS record present, even longer historical accounts of large earthquakes (including rupture locations), and even seafloor observations.
- We are exploring the **possibility of using GPUs** to speed up the computations.
- We are exploring options to **validate our code** with other, more detailed earthquake cycle codes.

References

[1] Agata, R., Barbot, S. D., Fujita, K., Hyodo, M., Iinuma, T., Nakata, R., et al. (2019). *Rapid mantle flow with power-law creep explains deformation after the 2011 Tohoku mega-quake.* Nature Communications, 10(1), 1385.

[2] Blanpied, M. L., Lockner, D. A., & Byerlee, J. D. (1995). Frictional slip of granite at hydrothermal conditions. Journal of Geophysical Research: Solid Earth, 100(B7), 13045–13064.

[3] Freed, A. M., Hirth, G., & Behn, M. D. (2012). *Using short-term postseismic displacements to infer the ambient deformation conditions of the upper mantle.* Journal of Geophysical Research: Solid Earth, 117(B1).

[4] Fukuda, J., & Johnson, K. M. (2021). *Bayesian Inversion for a Stress-Driven Model of Afterslip and Viscoelastic Relaxation: Method and Application to Postseismic Deformation Following the 2011 MW 9.0 Tohoku-Oki Earthquake.* Journal of Geophysical Research: Solid Earth, 126(5).

[5] Hetland, E. A., & Simons, M. (2010). *Post-seismic and interseismic fault creep II: transient creep and interseismic stress shadows on megathrusts.* Geophysical Journal International, 181(1), 99–112.

[6] Hetland, E. A., Simons, M., & Dunham, E. M. (2010). *Post-seismic and interseismic fault creep I: model description.* Geophysical Journal International, 181(1), 81–98.

[7] Hirth, G. (2002). *Laboratory Constraints on the Rheology of the Upper Mantle.* Reviews in Mineralogy and Geochemistry, 51(1), 97–120.

[8] Hirth, G., & Kohlstedt, D. (2004). *Rheology of the Upper Mantle and the Mantle Wedge: A View from the Experimentalists.* In Inside the Subduction Factory (pp. 83–105). American Geophysical Union (AGU).

[9] Kanda, R. V. S., & Simons, M. (2010). *An elastic plate model for interseismic deformation in subduction zones.* Journal of Geophysical Research: Solid Earth, 115(B3).

[10] Mallick, R., Lambert, V., & Meade, B. (2022). *On the Choice and Implications of Rheologies That Maintain Kinematic and Dynamic Consistency Over the Entire Earthquake Cycle.* Journal of Geophysical Research: Solid Earth, 127(9).

[11] Minson, S. E., Simons, M., & Beck, J. L. (2013). *Bayesian inversion for finite fault earthquake source models I—theory and algorithm.* Geophysical Journal International, 194(3), 1701–1726.

[12] Montési, L. G. J. (2004). *Controls of shear zone rheology and tectonic loading on postseismic creep.* Journal of Geophysical Research: Solid Earth, 109(B10).

[13] Montési, L. G. J., & Hirth, G. (2003). *Grain size evolution and the rheology of ductile shear zones: from laboratory experiments to postseismic creep.* Earth and Planetary Science Letters, 211(1), 97–110.

[14] Muto, J., Moore, J. D. P., Barbot, S., Iinuma, T., Ohta, Y., & Iwamori, H. (2019). *Coupled afterslip and transient mantle flow after the 2011 Tohoku earthquake.* Science Advances, 5(9).

[15] Weiss, J. R., Qiu, Q., Barbot, S., Wright, T. J., Foster, J. H., Saunders, A., et al. (2019). *Illuminating subduction zone rheological properties in the wake of a giant earthquake.* Science Advances, 5(12).